Microscopic theory of dipole-exchange spin-wave excitations in ferromagnetic nanowires

T. M. Nguyen and M. G. Cottam
Department of Physics and Astronomy, University of Western Ontario, London, Ontario, Canada N6A 3K7
(Received 7 October 2004; published 9 March 2005)

A microscopic theory is developed for the spin-wave excitations in ferromagnetic nanowires. Both the long-range magnetic dipole-dipole interactions and the Heisenberg-exchange interactions between nearest neighbors are included in the Hamiltonian, as well as effects of an applied magnetic field, which may be directed parallel or perpendicular to the wire axis. Our formalism can be applied to ferromagnetic nanowires of arbitrary cross section to deduce both the energy spectrum of the discrete dipole-exchange spin-wave modes and the relative intensities as a function of position. The long-range dipole sums in the wire geometry are evaluated numerically and spin-wave calculations are presented for nanowires with approximately circular cross section. When the applied field is perpendicular to the wire axis, there is a canting of the net spin orientation away from the axis, and the magnetization is spatially nonuniform due to the dipolar interactions. We find that typically there are two phases and two distinct regimes of spin-wave behavior, corresponding to the applied field being less than or greater than a critical value.

DOI: 10.1103/PhysRevB.71.094406 PACS number(s): 75.30.Ds, 75.75.+a

I. INTRODUCTION

The dynamical properties of regular arrays of submicrometer-scale magnetic dots and wires are currently attracting great attention due to their interesting fundamental physics and potential technological applications.[1] Experimentally, laterally confined magnetic structures in submicrometer and nanometer scale can be fabricated by various methods. For example, arrays of magnetic strips with rectangular cross sections as well as rectangular prisms and cylindrical dots can be created by using lithographic patterning procedures. Static and dynamic properties of such systems have been studied intensively in recent years.[1–5] Another important category of magnetic nanowires is fabricated by electrodeposition into porous templates.[6–8] These templates consist of nanometer-wide cylindrical pores which allow one to create magnetic nanowires of uniform diameter with extremely large aspect ratios of length to diameter (as large as 10^3). Other methods which combine electrodeposition and electron-beam or x-ray lithography have also been applied to create template materials where the position of the nanopillars and the spacing between them can be controlled precisely.[9] In this case, the aspect ratio is smaller (typically less than 5), and therefore some structures may have properties of a system of magnetic nanodots.

In addition to the magnetotransport properties and dynamics of the magnetization reversal which have been investigated intensively in both experimental and theoretical models, the spin-wave excitations in low-dimensional magnetic systems are also of fundamental importance due to their role in defining the time scale of the magnetization reversal process. Also, other important information on magnetic properties, such as the homogeneity of the internal field, contributions due to magnetic anisotropy, and the dipolar interactions between magnetic elements can be obtained from spin-wave measurements.

The spin-wave (SW) excitations or small amplitude dynamics are usually investigated by ferromagnetic resonance or Brillouin light scattering (BLS). While the former is usually used to study the dependence of the uniform precession mode on the pumping field orientation,[10,11] the latter technique is employed extensively to investigate the excitation spectrum in laterally confined structures (see, e.g., Ref. 1). Recently, Wang *et al.*[12] have applied BLS to study SW excitations in highly ordered arrays of ferromagnetic nickel nanowires, fabricated by electrodeposition in Al_2O_3 templates.[7,8] The results reveal three quantized SW modes in dipole-exchange regime, which were strongly influenced by wire diameter and interwire coupling. More interestingly, the results show that when the external field is applied perpendicular to the wires, there exist two different phases of dynamical behavior corresponding to the applied field less than or greater than a critical value.

Theoretically, the dipole-exchange SW in ferromagnetic nanowires and nanodots have been studied by a number of authors.[14–17] For example, Arias and Mills[14] have applied the continuum model to develop a theory for spin waves in a long cylindrical ferromagnetic nanowire where the magnetization is assumed to be uniform and parallel to the wire axis. The theory has been applied successfully by Wang *et al.*[12] to explain their data at zero field. However, this theory cannot be extended to the transverse case where the external field is applied perpendicular to the wire as in the BLS experiments.[12] In this orientation, due to the dipole-dipole interactions the magnetization is canted relatively to the symmetry axes and distributed nonuniformly throughout the wire cross section. Also the macroscopic method, which depends on a continuum approximation, breaks down for sufficiently thin nanowires and/or for large SW wave vectors. This fact, plus the absence of a macroscopic theory in the transverse-field case, has motivated our present work.

In this paper we develop a microscopic theory for spin waves in ferromagnetic nanowires with approximately circular cross section. We concentrate on the regime where both exchange and dipolar interactions may provide comparable contributions to the dynamical processes. The operator

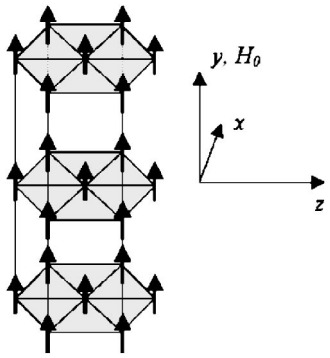

FIG. 1. A nanowire with $N=7$ in a longitudinal applied magnetic field.

method that we employ here is analogous to that developed in recent work on ultrathin films of ferromagnets[18] and antiferromagnets.[19]

The paper is arranged as follows. Section II describes the theoretical model for a cylindrical ferromagnetic nanowire. The Hamiltonian includes the exchange, dipolar, and Zeeman terms, where the external magnetic field is applied either parallel or perpendicular to the wire axis. Results for linear SW dispersion relation are then derived in Sec. III, where numerical examples are provided to illustrate the theory for the dependence of the discrete SW frequencies on wave vector, applied magnetic field and nanowire radius. Numerical results are also given for the spatial distribution of the mode intensities. In an appropriate limit of the general theory, we are also able to deduce in Sec. IV some preliminary results for arrays of nanowires with dipolar interwire coupling. Section V is devoted to further discussion and overall conclusions.

II. THEORETICAL MODEL

A nanowire can be modeled by specifying a cross-sectional layer (of a chosen shape and size) and then stacking these atomic layers vertically on one another to form a long nanowire with translational symmetry along the stacking direction. Specifically we consider here nanowires having a hexagonal cross section (in the xz plane), each with a finite number N spins arranged on a triangular lattice (spacing a). These layers are stacked vertically to form a long nanowire extending in the y direction from $-\infty$ to ∞. This geometry is illustrated in Fig. 1. The simplest case of $N=1$ corresponds to a single line of spins, whereas wires of "radius" ra (where $r=1,2,3,\ldots$) corresponds to $N=3r(r+1)+1=7,19,37$, etc. An external magnetic field of magnitude H_0 can be applied along or perpendicular to the wire axis, with the latter case allowing comparison with the experimental situation in Ref. 12. Thus the Hamiltonian can be expressed generally as

$$H=-\frac{1}{2}\sum_{in,jm} J_{in,jm}\mathbf{S}_{in}\cdot\mathbf{S}_{jm}-g\mu_B\mathbf{H}_0\cdot\sum_{in}\mathbf{S}_{in}$$
$$+\frac{1}{2}g^2\mu_B^2\sum_{in,jm}\sum_{\alpha,\beta}D_{in,jm}^{\alpha,\beta}S_{in}^{\alpha}S_{jm}^{\beta}. \quad (1)$$

Here i,j are layer indices, while n,m label the position of the spins in a particular layer. The exchange interaction between the spin operators at sites (i,n) and (j,m) is $J_{in,jm}$. For simplicity, the exchange will be taken to be J between nearest neighbors along the y direction, $J_\perp$ between nearest neighbors in the xz plane, and zero otherwise. The second term represents the Zeeman energy due to the external field, which can be applied parallel or perpendicular to the wire. The final term in Eq. (1) describes the long-range dipole-dipole interactions with the α and β labels denoting Cartesian components x, y, or z and

$$D_{in,jm}^{\alpha,\beta}=\frac{|\mathbf{r}_{in,jm}|^2\delta_{\alpha,\beta}-3r_{in,jm}^{\alpha}r_{in,jm}^{\beta}}{|\mathbf{r}_{in,jm}|^5}, \quad (2)$$

where $\mathbf{r}_{in,jm}=(x_m-x_n,y_j-y_i,z_m-z_n)$ and the case $(i=j,n=m)$ is excluded from the sums in Eq. (1).

In some cases we may want to take $J_\perp=J$ for the two exchange constants. In other cases (e.g., to model an array of 1D wires as in Sec. IV) we may choose to set $J_\perp=0$, so that interwire coupling is due to the dipolar term only. We now examine separately the distinct types of physical behavior obtained when the magnetic field is parallel or perpendicular to the y axis.

A. Longitudinal case

When the magnetic field is applied parallel to the wire, the magnetization is uniform and the equilibrium orientation of each spin is along the wire axis. In this case the approximate SW excitation spectrum can be calculated by using a macroscopic continuum model. In fact, SW theories for a long cylindrical ferromagnetic nanowire were developed by Sharon and Maradudin[13] and by Arias and Mills[14] using this method for the magnetostatic and dipole-exchange regimes, respectively. The latter theory was applied successfully by Wang *et al.*[12] to explain some of their experimental results at zero external field. As mentioned above, the microscopic theory is needed for small-diameter wires and/or for larger SW wave vectors, where a continuum approximation is unsatisfactory.

We start with the assumption that the equilibrium orientation of all the spins is along the y axis, which is parallel to the symmetry axis of the nanowire. To examine the SW properties at low temperatures $(T\ll T_c)$ we first transform the spin Hamiltonian into an equivalent form in boson operators. There are several ways to carry out this step, but in the present paper we use (following Refs. 18 and 19) the Holstein-Primakoff transformation. Corresponding to our choice of coordinate axes, the components of a spin vector $\mathbf{S}_{in}$ are represented in terms of boson creation and annihilation operators $a_{in}^{\dagger}$ and a_{in} by the expressions (denoting $S_{in}^{\pm}=S_{in}^{z}\pm iS_{in}^{x}$)

$$S_{in}^{+}=\sqrt{2S}(1-a_{in}^{\dagger}a_{in}/2S)^{1/2}a_{in}, \quad (3)$$

$$S_{in}^{-}=\sqrt{2S}a_{in}^{\dagger}(1-a_{in}^{\dagger}a_{in}/2S)^{1/2}, \quad (4)$$

$$S_{in}^{y}=S-a_{in}^{\dagger}a_{in}. \quad (5)$$

The transformed Hamiltonian can then be expanded, apart from a constant, as $H=H^{(1)}+H^{(2)}+H^{(3)}+H^{(4)}+\cdots$, where

$H^{(m)}$ denotes a term with m boson operators. The constant term has no role in dynamical properties while the first order term $H^{(1)}$ vanishes by symmetry in the present longitudinal-field case. The noninteracting (linear) SW excitations will be obtained from the quadratic Hamiltonian $H^{(2)}$. After making a 1D Fourier transform along the wire axis, it has the form

$$H^{(2)} = \sum_{k,n,m} \{A^{(2)}_{n,m}(k) a^{\dagger}_{k,n} a_{k,m} + B^{(2)}_{n,m}(k) a^{\dagger}_{k,n} a^{\dagger}_{-k,m} + B^{(2)*}_{n,m}(k) a_{k,n} a_{-k,m}\}, \quad (6)$$

where k is a wave number along the wire axis. The terms $H^{(3)}$ and $H^{(4)}$ describe leading-order effects of SW interactions and will not be considered further in the present paper.

In the above result we have written the boson operators $a^{\dagger}_{k,n}$ and $a_{k,m}$ in terms of k and the site indices n and m in a particular layer. The coefficients in Eq. (6) are given explicitly by

$$A^{(2)}_{n,m}(k) = \Delta_n \delta_{n,m} - S J_{n,m}(k) - \frac{1}{2} S (g\mu_B)^2 D^{y,y}_{n,m}(k), \quad (7)$$

$$B^{(2)}_{n,m}(k) = \frac{1}{4} S (g\mu_B)^2 \{D^{z,z}_{n,m}(k) - D^{x,x}_{n,m}(k) + 2i D^{x,z}_{n,m}(k)\}, \quad (8)$$

where

$$\Delta_n = g\mu_B H_0 + S \sum_l [J_{n,l}(0) - (g\mu_B)^2 D^{y,y}_{n,l}(0)]. \quad (9)$$

We have also introduced the 1D Fourier transforms $J_{n,m}(k)$ and $D^{\alpha,\beta}_{n,m}(k)$ of the exchange and dipole-dipole interactions respectively, defined, e.g., by

$$J_{n,m}(k) = \sum_j J_{in,jm} \exp[ik(y_i - y_j)]. \quad (10)$$

In the case of nearest-neighbor (NN) coupling the functions $J_{n,m}(k)$ have a simple form and are

$$J_{n,m}(k) = \begin{cases} 2J\cos(ka) & \text{if } n = m, \\ J_{\perp} & \text{if } n \text{ and } m \text{ are NN}, \\ 0 & \text{otherwise}. \end{cases} \quad (11)$$

As mentioned, to model a single composite nanowire of radius $R = ra$, we simply take $J_{\perp} = J$ in most of our numerical calculations. The functions $D^{\alpha,\beta}_{n,m}(k)$ are defined in an analogous way to Eq. (10). They are nonzero in general for all n and m, although they vanish by symmetry for some choices of α and β. They will later be evaluated numerically, taking care of their slow convergence in the y direction. In the Sec. III, we show how the Hamiltonian (6) can be diagonalized using a matrix method to obtain the linear SW spectrum.

B. Transverse case

We now consider the more interesting case where the external magnetic field is applied along the z axis, which is perpendicular to the wire. Due to the competition between the applied field and the demagnetizing field, the spins are canted relative to the symmetry axes and therefore the magnetization becomes spatially nonuniform. As a consequence we use a microscopic rather than macroscopic theory. We now assume that the equilibrium orientation of the spin at site (i,n) is characterized by two angles α_n and θ_n so that $\mathbf{S}_{in} = S(\sin\alpha_n \sin\theta_n, \cos\alpha_n, \sin\alpha_n \cos\theta_n)$, as represented in Fig. 2(a). The total free energy obtained from the Hamiltonian (1) can be written as

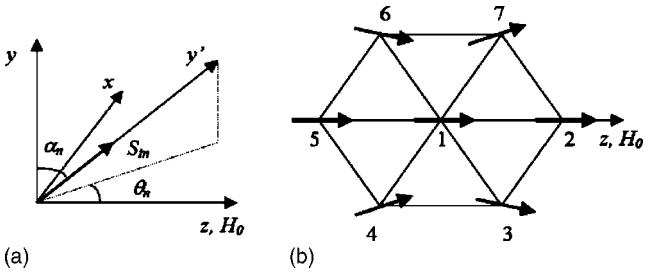

FIG. 2. Schematic view of the canted spins in a transverse applied magnetic field. (a) The spin $\mathbf{S}_{in}$ is canted relative to the global axes in the case of $H_0 < H_c$. (b) Cross section of a $N=7$ nanowire showing the canted spins in the case of $H_0 > H_c$.

$$\begin{aligned} E = &-\frac{1}{2} S^2 L \sum_{n,m} J_{n,m}(0)[\sin\alpha_n \sin\theta_n \sin\alpha_m \sin\theta_m \\ &+ \cos\alpha_n \cos\alpha_m + \sin\alpha_n \cos\theta_n \sin\alpha_m \cos\theta_m] \\ &- g\mu_B H_0 S \sum_n \sin\alpha_n \cos\theta_n \\ &+ \frac{1}{2}(g\mu_B)^2 S^2 L \sum_{n,m} [D^{x,x}_{n,m}(0)\sin\alpha_n \sin\theta_n \sin\alpha_m \sin\theta_m \\ &+ D^{y,y}_{n,m}(0)\cos\alpha_n \cos\alpha_m \\ &+ D^{z,z}_{n,m}(0)\sin\alpha_n \cos\theta_n \sin\alpha_m \cos\theta_m \\ &+ 2D^{x,z}_{n,m}(0)\sin\alpha_n \sin\theta_n \sin\alpha_m \cos\theta_m], \end{aligned} \quad (12)$$

where L is the (macroscopically large) number of layers along the wire. We have chosen the coordinate system such that the y axis is parallel to the wire, which implies $D^{x,y}_{n,m}(0) = D^{y,z}_{n,m}(0) = 0$. In order to minimize E the canting angles $\{\alpha_n, \theta_n\}$ must satisfy the conditions

$$\delta E/\delta\alpha_n = 0 \quad \text{and} \quad \delta E/\delta\theta_n = 0, \quad (13)$$

which yield (for $n = 1, 2, \ldots, N$)

$$\begin{aligned} &g\mu_B H_0 \cos\alpha_n \cos\theta_n + S \sum_m J_{n,m}(0) \\ &\times[\cos\alpha_n \sin\theta_n \sin\alpha_m \sin\theta_m - \sin\alpha_n \cos\alpha_m \\ &+ \cos\alpha_n \cos\theta_n \sin\alpha_m \cos\theta_m] \\ &- (g\mu_B)^2 S \sum_m [D^{x,x}_{n,m}(0)\cos\alpha_n \sin\theta_n \sin\alpha_m \sin\theta_m \\ &- D^{y,y}_{n,m}(0)\sin\alpha_n \cos\alpha_m \\ &+ D^{z,z}_{n,m}(0)\cos\alpha_n \cos\theta_n \sin\alpha_m \cos\theta_m \\ &+ D^{x,z}_{n,m}(0)\cos\alpha_n \sin\alpha_m \sin(\theta_n + \theta_m)] = 0 \end{aligned} \quad (14)$$

and

$$\sin\alpha_n\Big[g\mu_B H_0\sin\theta_n - S\sum_m J_{n,m}(0)\{\cos\theta_n\sin\alpha_m\sin\theta_m - \sin\theta_n\sin\alpha_m\cos\theta_m\} + (g\mu_B)^2 S\sum_m \{D^{x,x}_{n,m}(0)\times\cos\theta_n\sin\alpha_m\sin\theta_m - D^{z,z}_{n,m}(0)\sin\theta_n\sin\alpha_m\cos\theta_m + D^{x,z}_{n,m}(0)\sin\alpha_m\cos(\theta_n+\theta_m)\}\Big] = 0. \quad (15)$$

By solving these coupled equations we can obtain the set of angles $\{\alpha_n,\theta_n\}$ that minimize the total free energy and hence determine the equilibrium configuration. Except in the case of $N=1$ (a single line of spins), this will require making an approximation, and we return to this matter later. To proceed with the SW calculation, the Holstein-Primakoff transformation is now applied relative to the *local* coordinates (x',y',z') assigned to each spin individually such that the y' axis is along the equilibrium direction of that spin. In term of the global coordinates (x,y,z), the transformations have the following form (retaining only those terms that will contribute to the linear SW approximation):

$$\begin{aligned} S^x_{in} &= S\sin\theta_n\sin\alpha_n + \sqrt{S/2}(\sin\theta_n\cos\alpha_n + i\cos\theta_n)a^\dagger_{in} \\ &\quad + \sqrt{S/2}(\sin\theta_n\cos\alpha_n - i\cos\theta_n)a_{in} \\ &\quad - \sin\theta_n\sin\alpha_n a^\dagger_{in}a_{in} + \cdots, \\ S^y_{in} &= S\cos\alpha_n - \sqrt{S/2}\sin\alpha_n(a^\dagger_{in}+a_{in}) - \cos\alpha_n a^\dagger_{in}a_{in} + \cdots, \\ S^z_{in} &= S\cos\theta_n\sin\alpha_n + \sqrt{S/2}(\cos\theta_n\cos\alpha_n - i\sin\theta_n)a^\dagger_{in} \\ &\quad + \sqrt{S/2}(\cos\theta_n\cos\alpha_n + i\sin\theta_n)a_{in} \\ &\quad - \cos\theta_n\sin\alpha_n a^\dagger_{in}a_{in} + \cdots. \end{aligned} \quad (16)$$

We now substitute the transformation (16) into the Hamiltonian (1) and expand it in terms of boson operators as was done for the longitudinal case. As a consequence of Eq. (13) the first order term $H^{(1)}$ is found to vanish. The quadratic Hamiltonian $H^{(2)}$, after a 1D Fourier transform with respect to the global y coordinate, is represented by the same formal expression as Eq. (6). The modified coefficients $A^{(2)}_{n,m}(k)$ and $B^{(2)}_{n,m}(k)$ now depend on the canting angles $\{\alpha_n,\theta_n\}$ and they are quoted in the Appendix. Information about the linear SW spectrum will next be obtained directly by diagonalizing the quadratic Hamiltonian, following an analysis of the longitudinal case.

III. SPIN-WAVE DISPERSION RELATIONS

A. Longitudinal case

In order to obtain the linear SW spectrum, the quadratic Hamiltonian (6) must be diagonalized. This can be done by applying a generalized Bogoliubov transformation, and thus following Refs. 18 and 20 we first rewrite the quadratic Hamiltonian $H^{(2)}$ in matrix form as

$$H^{(2)} = -\frac{1}{2}\sum_k \mathrm{Tr}[\mathbf{A}(k)] + \frac{1}{2}\sum_k \tilde{\mathbf{C}}^+_k\mathbf{F}(k)\mathbf{C}_k, \quad (17)$$

where

$$\mathbf{F}(k) = \begin{pmatrix} \mathbf{A}(k) & 2\mathbf{B}(k) \\ 2\mathbf{B}^*(-k) & \tilde{\mathbf{A}}(-k) \end{pmatrix}, \quad (18)$$

with the tilde denoting a transpose matrix. Here $\mathbf{A}(k)$ and $\mathbf{B}(k)$ are $N\times N$ matrices with elements given by the coefficients $A^{(2)}_{n,m}$ and $B^{(2)}_{n,m}$ of the Hamiltonian $H^{(2)}$, respectively, and we have also defined operators $\mathbf{C}^+_k$ and $\mathbf{C}_k$ as

$$\mathbf{C}^+_k = \begin{pmatrix} a^+_k \\ a_{-k} \end{pmatrix}, \quad \mathbf{C}_k = \begin{pmatrix} a_k \\ a^+_{-k} \end{pmatrix}, \quad (19)$$

where a^+_k and a_k are N-component column matrices with their nth elements equal to $a^\dagger_{k,n}$ and $a_{k,n}$, respectively.

The first term in Eq. (17) is just a constant, while the second term can be diagonalized to provide the noninteracting SW spectrum. To achieve this we introduce a new set of boson operators b^+_k and b_k, which satisfy the usual commutation relations and are defined by

$$a_{k,n} = \sum_{m=1}^{N} S_{n,m}(k)b_{k,m} + S_{n,m+N}(k)b^\dagger_{-k,m}, \quad (20)$$

$$a^\dagger_{-k,n} = \sum_{m=1}^{N} S_{n+N,m}(k)b_{k,m} + S_{n+N,m+N}(k)b^\dagger_{-k,m}, \quad (21)$$

where $S_{n,m}(k)$ is an element of the $2N\times 2N$ transformation matrix $\mathbf{S}_k$. The transformation can be written in matrix form as $\mathbf{C}_k=\mathbf{S}_k\mathbf{D}_k$ and $\mathbf{C}^+_k=\mathbf{S}^*_k\mathbf{D}^+_k$, where $\mathbf{D}_k$ and $\mathbf{D}^+_k$ are defined similarly to $\mathbf{C}_k$ and $\mathbf{C}^+_k$ but in terms of the new boson operators. The lth column of the matrix $\mathbf{S}_k$, which we denote by $\mathbf{S}_l(k)$, as well as the noninteracting SW frequencies, which we denote by $\omega_{k,l}$, can be found by solving the following eigenvalue equation:

$$\begin{pmatrix} \mathbf{A}(k) & 2\mathbf{B}(k) \\ -2\mathbf{B}^*(-k) & -\tilde{\mathbf{A}}(-k) \end{pmatrix}\mathbf{S}_l(k) = \pm\omega_{k,l}\mathbf{S}_l(k), \quad (22)$$

where the $+$ sign is taken for $l=1,\ldots,N$ and the $-$ sign for $l=N+1,\ldots,2N$. The quadratic Hamiltonian then assumes the diagonalized form given by

$$H^{(2)} = -\frac{1}{2}\sum_k \mathrm{Tr}[\mathbf{A}(k)] + \frac{1}{2}\sum_{k,l=1}^{N}\omega_{k,l} + \sum_{k,l=1}^{N}\omega_{k,l}b^\dagger_{k,l}b_{k,l}. \quad (23)$$

Some numerical examples are now presented to illustrate this theory. In particular, we show dispersion relation for $\omega_{k,l}$ versus wave vector k for the N branches $(l=1,\ldots,N)$. Nu-

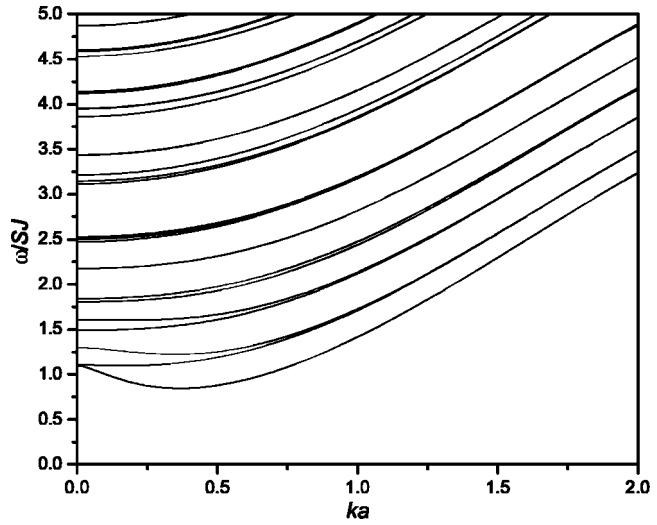

FIG. 3. SW frequency versus wave number ka for a nanowire with $N=91$ in a longitudinal applied field, taking $J_\perp = J$, $h=0.5$, and $R_d=0.1$.

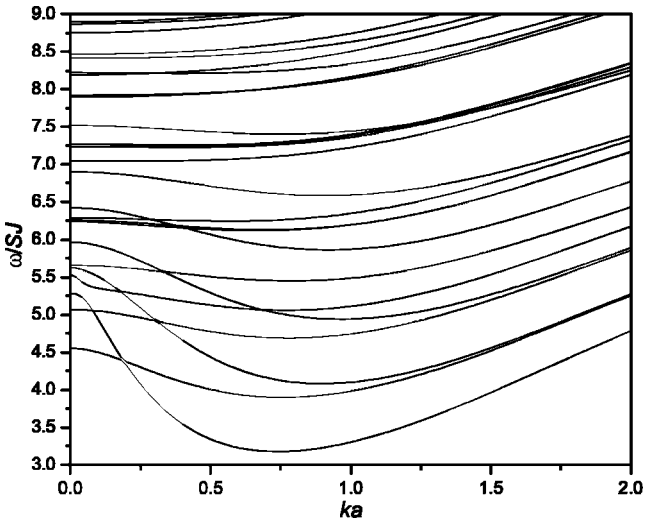

FIG. 4. The same as in Fig. 3, but taking $h=2.5$ and $R_d=0.5$.

merical calculations are carried out for the reduced frequency ω/SJ in terms of two dimensionless parameters

$$h = g\mu_B H_0/SJ \text{ and } R_d = (g\mu_B)^2/Ja^3, \tag{24}$$

where the latter measures the relative strengths of the dipolar and exchange interactions.

For a general description of SW dispersion relation, we first consider nanowires with the effective radius (in units of a) of $r=1$ and $r=5$, corresponding to $N=7$ and $N=91$, respectively. Note that the lattice constant a is an effective value and the spin **S** at each "lattice" site may be chosen to represent either a single spin or a "cluster" of spins. We will discuss later how the values of a and R_d may be selected in order to make comparisons with real nanowires. Calculations have been performed using a stand-alone Pentium PC to study nanowires with radius up to $r=20$ (corresponding to $N=1261$).

In Fig. 3, for $R_d=0.1$ and $h=0.5$, we show just the lowest of the N discrete SW modes in a nanowire with $N=91$. Some of the modes show a minimum at nonzero wave vector, arising as a consequence of interplay between the dipolar and exchange interactions. This feature has been pointed out within a continuum model by Arias and Mills,[14] who evaluate the dipolar contribution to the dispersion at small values of the wave vector. At small values of ka (e.g., where either the wave length or the nanowire radius is much larger than the so-called exchange length), the magnetic dipolar interaction and the effect of the boundary confinement are large compared to the influence of the exchange interaction. This leads to a decrease of the lowest SW frequencies with increasing ka, which is similar to the behavior found for magnetostatic modes in the wire geometry.[13] At larger values of ka, the exchange interaction dominates and the SW frequencies increase. Figure 4 is similar to Fig. 3, but for $R_d=0.5$ and $h=2.5$. Here we have fixed the ratio of h to R_d to be equal to 5, so that in effect the only parameter which we really vary is the length scale a, and therefore the nanowire radius. The SW frequencies show not only a minimum for the lowest curves at nonzero wave vector as in Fig. 3, but also there is strong evidence of mode-repulsion effects in the range of small ka. For comparison, we note that in the case of a thin film with in-plane magnetization similar features have been observed when the SWs are propagating normally to the direction of magnetization.[21,22] The mode repulsion might be interpreted as a manifestation of the strong confinement effects which result in a mixing of the magnetostatic (dipolar) surface mode with the lowest-lying perpendicular standing SW modes.

We note that information about the spatial distribution of relative intensities of normal modes can be deduced from the transformation matrix $\mathbf{S}_k$. More precisely, we introduce

$$P_n(\omega_{k,l}) = \sqrt{|S_{n,l}(k)|^2 + |S_{n+N,l}(k)|^2} \tag{25}$$

as defining the probability amplitude for the mode with frequency $\omega_{k,l}$ propagating along the nth spin line. To illustrate this concept, we present here some numerical results for a simple case of a nanowire with $N=7$ in zero applied magnetic field. The spins in each cross section are numbered as indicated in Fig. 2(b). The corresponding SW frequencies as functions of wave vector are shown in Fig. 5, taking $R_d=0.1$. There are seven modes as expected, which we number in increasing value of the frequency. Note that there are near degeneracies between the second and third modes, and between the fourth and fifth modes. The relative intensities and their spatial dependence, as measured by $P_n(\omega_{0,l})$ for $n=1,2,\ldots,7$, are represented in Table I, where we choose wave number $k=0$ and the results are quoted for all seven modes. From this table we can see that the lowest mode is distributed almost uniformly among the spin lines, while the highest mode is concentrated mainly on the center line. The relative intensities of the second, third, and the sixth modes have identical pattern and are distributed equally between the outer lines.

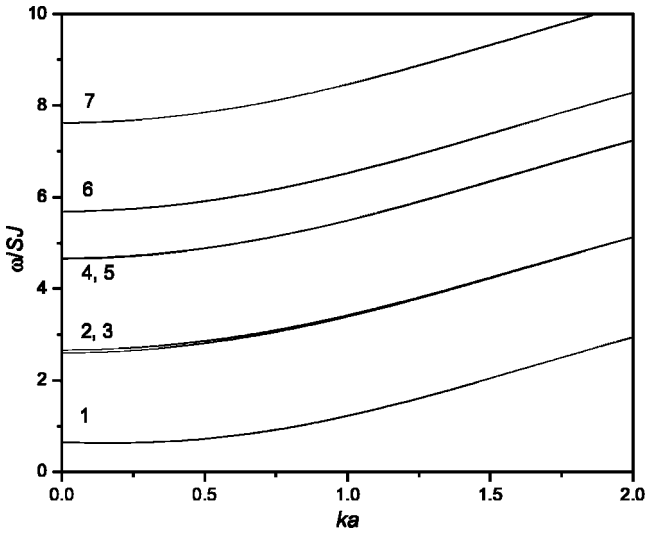

FIG. 5. SW frequency versus wave number ka for a nanowire with $N=7$ in zero applied magnetic field, taking $J_\perp = J$ and $R_d = 0.1$. The numbering of the modes is indicated.

In this particular example, where N is relatively small, we can usefully make comparisons with analytic results which we obtained in an exchange-dominated limit. We find in this limit that the SW frequencies at $k=0$ correspond simply to $\omega/SJ = 0,2,2,4,4,5,7$ in ascending order. This, together with the degeneracy scheme, is very similar to the behavior depicted in Fig. 5, except that the dipolar terms have led to an upward shift (of order 0.7 at $k=0$). Moreover, for the spatial distribution in the exchange limit, we find that the lowest SW mode (mode 1) has equal intensity at all sites n, and this is similar to Table I. Also the highest SW mode (mode 7) is found to have essentially the same intensity distribution irrespective of the inclusion of dipole-dipole interactions. This is because exchange effects are particularly important for mode 7. The SW modes 2 to 6 have zero intensity at $n=1$ in the exchange limit, and this similar overall behavior is found in Table I where the dipole-dipole effects are included.

B. Transverse case

The same matrix formalism to diagonalize $H^{(2)}$ can be applied in the transverse field case also. Thus Eqs. (17)–(23) are still valid, provided the appropriate form of the $A^{(2)}_{n,m}(k)$ and $B^{(2)}_{n,m}$ in Eqs. (A1) and (A2) are substituted. However, to carry through with this calculation, it is a necessary first step to determine the equilibrium configuration. As mentioned before, the equilibrium configuration is characterized by the set of angles $\{\alpha_n, \theta_n\}$. These angles can be obtained by solving numerically the nonlinear equations (14) and (15) as described below.

We first obtain an approximate analytic solution. Using the fact that the azimuthal angles $\{\theta_n\}$ relative to the magnetic field direction are very small in most cases, we can linearize Eq. (15), which becomes

$$g\mu_B H_0 \theta_n - S\sum_m \sin\alpha_m \{J_{n,m}(0)(\theta_m - \theta_n) + (g\mu_B)^2 [D^{x,x}_{n,m}(0)\theta_m - D^{z,z}_{n,m}(0)\theta_n + D^{x,z}_{n,m}(0)]\} = 0. \tag{26}$$

The polar angles $\{\alpha_n\}$ can then be approximated from Eq. (14) by assuming that $\alpha_n \simeq \alpha$ for every n. Neglecting small terms in θ_n we obtain

$$\sin\alpha = \begin{cases} h/h_c \text{ if } h < h_c, \\ 1 \text{ otherwise}, \end{cases} \tag{27}$$

where $h_c = g\mu_B H_c / SJ$ defines a critical field H_c. Its approximate value is

$$h_c \simeq \frac{R_d a^3}{N} \sum_{n,m} [D^{z,z}_{n,m}(0) - D^{y,y}_{n,m}(0)]. \tag{28}$$

The linear equations (26) for $\{\theta_n\}$ can be solved numerically by using standard methods, and they are found to depend on n. We note that the critical field given by Eq. (28) represents the demagnetizing field caused by a transverse component of the magnetization. In the continuum model, H_c is approximated as $2\pi M_s$, where M_s is the saturation magnetization (in our notation $M_s = \eta g\mu_B S/a^3$, where η is a scalar factor of order unity).

In a more precise calculation we use the values of $\{\alpha_n\}$ approximated by Eq. (27) and $\{\theta_n\}$ values obtained from solving the linear equations (26) as trial solutions to solve Eqs. (14) and (15) numerically in an iterative approach. The critical field h_c can also be evaluated numerically to justify the approximation made in obtaining Eq. (28). We assume

TABLE I. Relative intensities of SW resonance frequencies (at $k=0$) in a nanowire with $N=7$, taking $J_\perp = J$, $R_d = 0.1$, and $h=0$.

n	$P_n(\omega_{0,1})$	$P_n(\omega_{0,2})$	$P_n(\omega_{0,3})$	$P_n(\omega_{0,4})$	$P_n(\omega_{0,5})$	$P_n(\omega_{0,6})$	$P_n(\omega_{0,7})$
1	0.382	0.000	0.000	0.046	0.001	0.000	0.924
2	0.377	0.408	0.408	0.420	0.396	0.408	0.157
3	0.377	0.408	0.408	0.402	0.414	0.408	0.157
4	0.377	0.408	0.408	0.402	0.414	0.408	0.157
5	0.377	0.408	0.408	0.420	0.396	0.408	0.157
6	0.377	0.408	0.408	0.402	0.414	0.408	0.157
7	0.377	0.408	0.408	0.402	0.414	0.408	0.157

that when $h > h_c$ the demagnetizing fields are compensated and all the spins are canted perpendicular to the wire axis (although the θ_n angles will still vary). As the applied field h approaches the value h_c from below, the polar angles approach $\pi/2$ and therefore can be written as $\alpha_n = \pi/2 - \delta_n$, where $\delta_n \ll \pi/2$. Equation (14) can then be linearized with respect to $\{\delta_n\}$, as well as θ_n, and it has the following form in leading order:

$$C_{n,n}\delta_n + \sum_{m\neq n} C_{n,m}\delta_m = 0, \tag{29}$$

where

$$C_{n,n} = g\mu_B H_c + S\sum_{m\neq n} J_{n,m}(0) + (g\mu_B)^2 S\Big[D^{y,y}_{n,n}(0) - \sum_m D^{z,z}_{n,m}(0)\Big], \tag{30}$$

$$C_{n,m} = -SJ_{n,m}(0) + (g\mu_B)^2 S D^{y,y}_{n,m}(0), \quad n \neq m. \tag{31}$$

The value of h_c is then extracted numerically from the requirement that $\det(\mathbf{C}) = 0$, which is the condition for the nontrivial solution exists. For example, for nanowires with $N = 7$, 19, 37, 61, and 91, and choosing $R_d = 0.1$, we get $h_c/R_d = 6.48$ (6.46), 6.27 (6.24), 6.18 (6.14), 6.13 (6.09), and 6.11 (6.05), respectively. The values in parentheses are the approximate values given by Eq. (28), and all values are seen to be close to the 2π of the continuum theory.

As in the longitudinal case, we carry out numerical calculations for the reduced SW frequency ω/SJ in terms of wave number k and the two dimensionless parameters h and R_d defined in Eq. (24). We consider here a nanowire having effective radius of $r = 4$ (in unit of a), corresponding to $N = 61$. The value of R_d is chosen to be 0.1 in all the calculations.

The lowest branches of the SW resonance frequencies (at $k = 0$) are shown versus the applied magnetic field in Fig. 6. The most significant feature is that all the curves have a sharp minimum at the critical field $h_c = 0.613$, and the spin waves show distinct behavior for the applied field being less than or greater than this value. At larger values of applied field, the spins are perpendicular to the wire axis, and the SW frequencies increase monotonically (mainly due to the Zeeman energy term). The behavior of the SW modes is also interesting for the small values of H_0. In this case the spins are canted slightly with respect to the wire axis. The contribution of the Zeeman energy to the SW modes is overwhelmed by the demagnetizing energy and the curves decrease slowly with increasing field. Note that the lowest mode has a very sharp minimum but the frequency does not vanish. We interpret this as a consequence of nonuniform magnetization. As the spins are canted relative to the direction of applied field, though the canting angles θ_n are small, the exchange energy contained in the mode becomes greater than the demagnetizing energy. A qualitatively similar behavior to that in Fig. 6 has been observed in ferromagnetic films and multilayers with large out-of-plane anisotropy, as we shall discuss later.

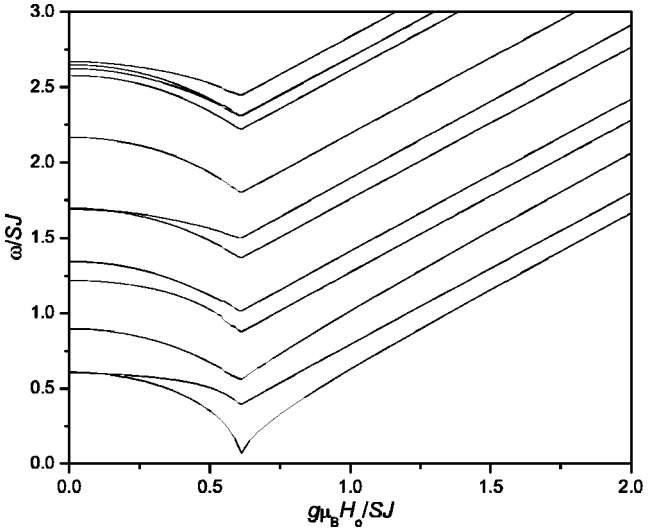

FIG. 6. SW frequency (at $k = 0$) versus transverse applied field for a nanowire with $N = 61$, taking $J_\perp = J$ and $R_d = 0.1$.

In Fig. 7 we show the frequencies of the lowest SW branches plotted versus ka, choosing the applied field $h = 0.3$, which is less than the critical value. Similarly to the longitudinal case, the lowest curve also has a minimum at a nonzero value of wave vector. Figure 8 is similar to Fig. 7, but for the applied field $h = 0.8$ which is greater than the critical value. In this case, the direction of propagation of the SW is perpendicular to the magnetization. Note that there is a precursor of a mode-repulsion effect at $ka \sim 0.2$ for the lowest curves, and no minima occur at nonzero ka. The curves increase monotonically with increasing ka.

IV. DIPOLE-COUPLED ARRAYS

In the previous sections, we have calculated the SW dispersion relation of a single, isolated nanowire. However,

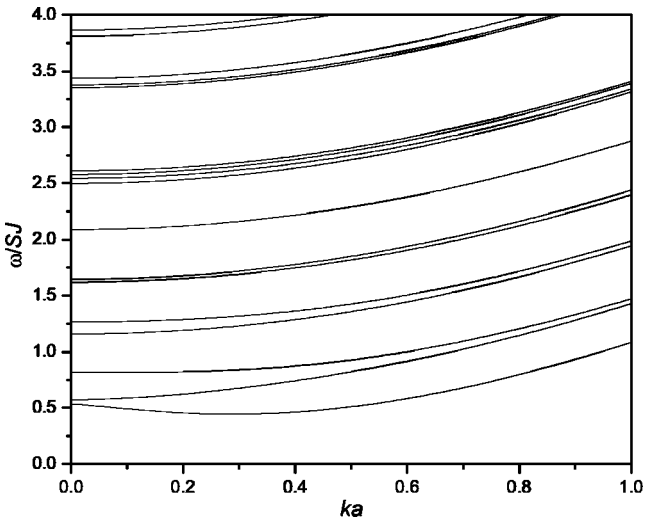

FIG. 7. SW frequency versus wave number ka for a nanowire with $N = 61$ in a transverse applied field, taking $J_\perp = J$, $h = 0.3$ ($< h_c$), and $R_d = 0.1$.

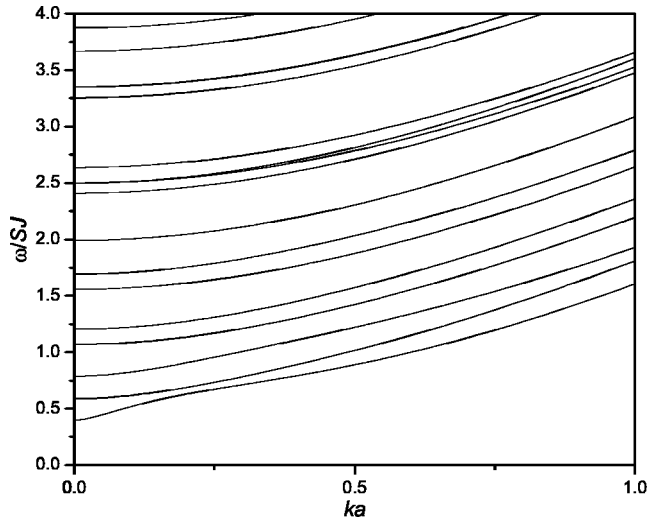

FIG. 8. The same as in Fig. 7, but taking $h=0.8$ ($>h_c$) and $R_d=0.1$.

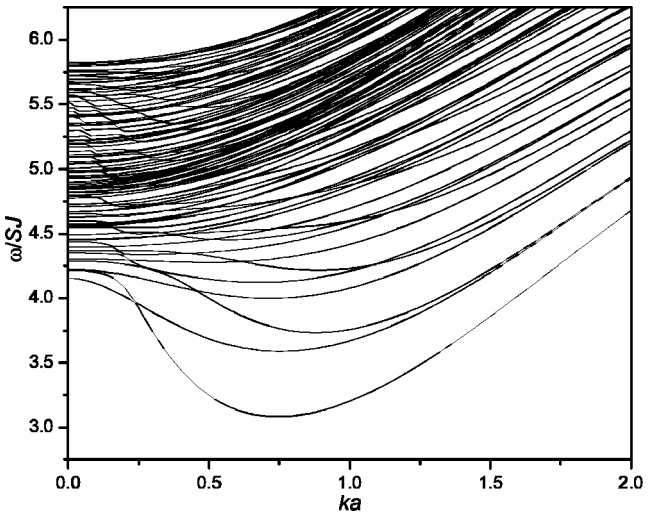

FIG. 9. SW frequency versus wave number ka for a nanowire array with $N=91$ in a longitudinal applied field, taking $J_\perp=0$, $h=2.5$, and $R_d=0.5$.

nanowire arrays fabricated using a method of combining lithography and electrodeposition techniques might be very dense, where the interwire distances as well as wire diameters can be controlled as desired. Also, the systems can be made to be ordered or disordered by varying the porosity of the templates. In such cases the dipolar interactions between wires may have significant effects on the SW spectrum.[10–12]

As mentioned earlier, we can choose to set $J_\perp=0$ to model an array of nanowires with dipolar interwire couplings. Here each wire is represented by a single line of spins. This simple model is aimed to describe the problem of ferromagnetic nanowires incorporated into a dense array. In the experiments carried out by Wang *et al.*[12] the nanowire arrays were, in fact, arranged in a hexagonal lattice, as in our theoretical model.

The results for the SW frequencies versus ka in the longitudinal case are presented in Fig. 9, taking the same parameters as in Fig. 4. We see that the behavior of the lowest curves is similar as in Fig. 4, but the upper curves are dramatically reduced in frequency, as expected, since there is no interwire exchange energy. The frequencies of SW resonance (at $k=0$) become almost a quasicontinuum. The repulsion of modes is also evident, though it is now more subtle.

We next present results for the SW frequencies of a nanowire array in a transverse applied field. It is, however, more complicated than the longitudinal case because the magnetic moments are canted from the symmetry axes and the demagnetizing field may cause the formation of domains in the xz plane. We first consider the case of $N=61$. The applied field is chosen as $h=1.2$, which is strong enough to overcome the demagnetizing fields. The results of SW frequencies versus ka are presented in Fig. 10. Note that the frequencies of all curves increase monotonically with increasing ka. This is because the propagation direction of the SW are perpendicular to the magnetization, so that the influence of dipole-dipole interactions becomes very weak and the k dependence is dominated by the intrawire exchange interaction. Another interesting feature that one can note from the figure is that the highest two modes are nearly degenerate with one another and are split off from a quasicontinuum formed by lower modes. This effect is similar to the case of splitting of optical surface modes from a band of bulk modes in a ferromagnetic slab.[22] To investigate the dependence of the SW resonance frequencies of a nanowire array on the magnitude of the applied field, it is appropriate to consider samples with small N in order to avoid here the possible formation of domain walls. The results for the case of $N=7$ are given in Fig. 11, taking $R_d=0.1$. Note that the four lowest modes go soft near the critical field. This type of phenomenon has been observed in ferromagnetic thin films and multilayers with out-of-plane anisotropies by Stamps and Hillebrands,[23,24] who made applications to Co/Pd and Co/Pt superlatices. The mode-repulsion effect are evident in our calculations for applied fields both below and above h_c.

As in the previous sections, the question again arises of how the intensities of the SW modes of a nanowire array are

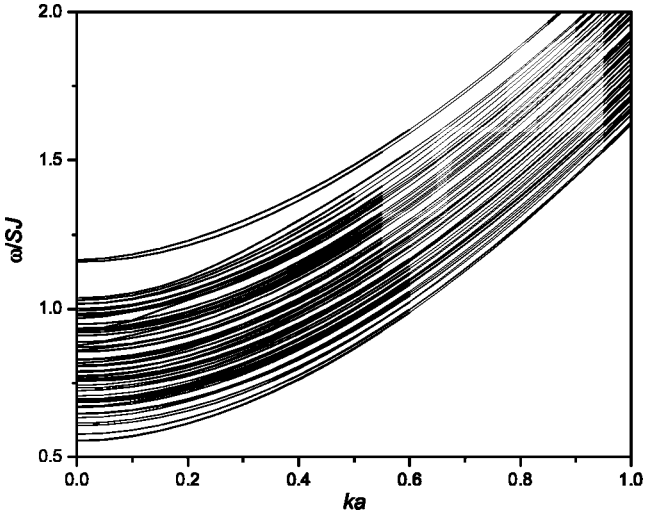

FIG. 10. SW frequency versus wave number ka for a nanowire array with $N=61$ in a transverse applied field, taking $J_\perp=0$, $h=1.2$ ($>h_c$), and $R_d=0.1$.

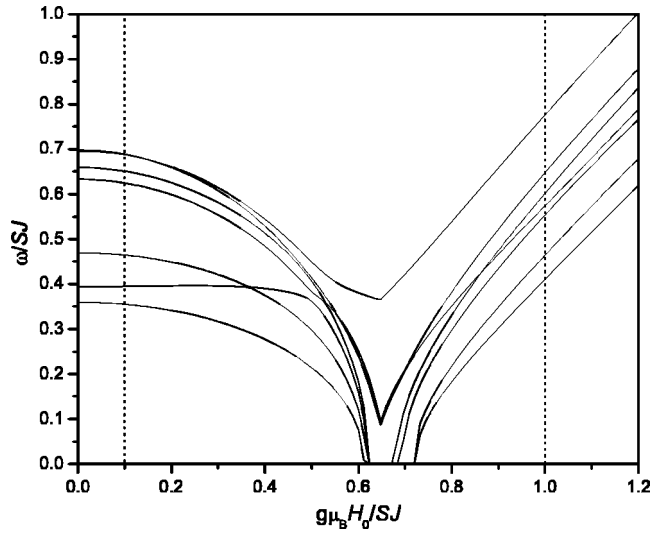

FIG. 11. SW frequency (at $k=0$) versus transverse applied field for a nanowire array with $N=7$, taking $J_\perp=0$ and $R_d=0.1$.

distributed among the wires (i.e., their spatial dependence). To have a qualitative understanding, we evaluate numerically the probability amplitude $P_n(\omega_{0,l})$. This was defined in Eq. (25) and it provides a measure of the intensity for the resonance mode $\omega_{0,l}$ propagating along the nth wire. Results for the case of a nanowire array with $N=7$ are presented in Tables II and III for $h=0.1$ ($h<h_c$) and 1.0 ($h>h_c$), respectively. The behavior is seen to be quite distinct in the two cases, due to the different equilibrium configurations of the spins.

V. DISCUSSION AND CONCLUSIONS

We have developed a microscopic theory describing the dipole-exchange SW excitations in a single ferromagnetic nanowire and/or arrays of these nanowires. The two different cases of external magnetic fields applied parallel or perpendicular to the wires have been treated separately. In the longitudinal case, the magnetization is uniform and directed along the symmetry axis. This fact simplifies the problem, and one can obtained the SW spectrum by applying the Holstein-Primakoff transformation directly to the Hamiltonian. Our results are qualitatively in agreement with results of the macroscopic theory developed by Arias and Mills[14] in the appropriate limiting cases. Moreover, from the theory we are able to investigate in detail the relative intensities of each discrete SW mode, which is spatially distributed among the spin lines.

The case of transverse applied field is more complicated because one needs to take into account the effects of nonuniform magnetization. We first find the equilibrium configuration of spins by minimizing the classical free energy, which is deduced from the microscopic Hamiltonian, with respect to the canting angles of spins. The Holstein-Primakoff transformation is now applied to the *local* coordinates of each spins. The SW spectrum is obtained following the diagonalization procedure used in the longitudinal case. The dependence of SW resonance frequencies on the magnitude of the applied field has been investigated, showing that there is a sharp minimum of all frequency curves at a critical value h_c, and the behavior of the SW is different for the applied field being less than or greater than this value. This feature is characteristic of unsaturated ferromagnetic systems,[21] where there is a strong competition between the exchange and the demagnetizing energies. Also, when the direction of the external magnetic field is not parallel to the easy axis, the magnetization will deviate from the easy axis and eventually line up with the applied field. The demagnetizing energy, which is proportional to the magnetization component in the direction of applied field, will first decrease with increasing magnetic field and reach its minimum when the magnetization is in the direction of applied field. This adds up with the monotonically increasing Zeeman and exchange energies to result in a sharp minimum of the SW frequency curves as we mentioned before. The value of h_c is found to decrease slightly with increasing wire radius. In a case of nanowire arrays when the interwire exchange interactions are switched off, the lowest modes go soft in a range of applied field around h_c.

In the calculations, we have been using a model of nanowires having hexagonal cross section. The aim here is to mimic the experimental situation,[12] where arrays of metallic ferromagnetic nanowires of circular cross section were employed. As mentioned before, the lattice constant a in any realistic application is an effective value and needs to be chosen appropriately for a particular nanowire. The exchange coupling J, or more precisely SJ, will be scaled accordingly, provided that the exchange stiffness $D=SJa^2/g\mu_B$ is known.

TABLE II. Relative intensities of SW resonance frequencies (at $k=0$) in a nanowire array with $N=7$, taking $J_\perp=0$, $R_d=0.1$, and $h=0.1$ ($<h_c$).

n	$P_n(\omega_{0,1})$	$P_n(\omega_{0,2})$	$P_n(\omega_{0,3})$	$P_n(\omega_{0,4})$	$P_n(\omega_{0,5})$	$P_n(\omega_{0,6})$	$P_n(\omega_{0,7})$
1	0.000	0.903	0.416	0.058	0.000	0.070	0.000
2	0.436	0.182	0.436	0.424	0.519	0.269	0.157
3	0.394	0.172	0.334	0.399	0.339	0.461	0.488
4	0.394	0.172	0.334	0.399	0.339	0.461	0.488
5	0.436	0.182	0.436	0.424	0.519	0.269	0.157
6	0.394	0.172	0.334	0.399	0.339	0.461	0.488
7	0.394	0.172	0.334	0.399	0.339	0.461	0.488

TABLE III. The same as in Table II, but taking $h=1.0$ ($>h_c$).

n	$P_n(\omega_{0,1})$	$P_n(\omega_{0,2})$	$P_n(\omega_{0,3})$	$P_n(\omega_{0,4})$	$P_n(\omega_{0,5})$	$P_n(\omega_{0,6})$	$P_n(\omega_{0,7})$
1	0.000	0.000	0.188	0.642	0.000	0.000	0.722
2	0.162	0.000	0.066	0.519	0.000	0.676	0.475
3	0.487	0.500	0.489	0.110	0.500	0.147	0.081
4	0.487	0.500	0.489	0.110	0.500	0.147	0.081
5	0.162	0.000	0.066	0.519	0.000	0.676	0.475
6	0.487	0.500	0.489	0.110	0.500	0.147	0.081
7	0.487	0.500	0.489	0.110	0.500	0.147	0.081

Also, the connection between the microscopic and macroscopic theories can be inferred from the definition of the magnetization $M_s=\eta g\mu_B S/a^3$, where η is a geometrical factor (of order unity) depending on the lattice structure. In our model, $\eta=[3r(r+1)+1]/(\pi r^2)$. The parameters R_d and h can be written in terms of D and M_s as follows:

$$R_d = M_s a^2/\eta D, \tag{32}$$

$$h = H_0 a^2/D. \tag{33}$$

Knowing the values of D and M_s of a particular nanowire, we can then choose the parameter R_d appropriately. For example, a nickel nanowire of radius $R=25$ nm as studied by Wang *et al.*[12] can be modeled as having $a=5$ nm and $r=5$, corresponding to $N=91$. Using values of the magnetization $M_s\simeq 0.0480$ T and the exchange stiffness $D\simeq 3.13\times 10^{-14}$ T cm^2,[12] the effective parameter R_d can be deduced approximately as $R_d\simeq 0.33$ while $h=1$ corresponding to the applied field $H_0\simeq 0.13$ T. Also, taking $g\mu_B=28$ GHz/T the *scaled* value of SJ (in frequency units) is ~ 3.5 GHz.

In order to have quantitative comparison with experiments, one needs to calculate the distribution of relative integrated intensities among the discrete SW modes, which requires obtaining the spin-correlation functions. For example, in the Brillouin scattering data of Ref. 12, the SW were observed in three broad bands of frequency. Within our formalism, this can be done by calculating the spin-spin Green's functions corresponding to the Hamiltonian (1) and we intend to address this problem in future studies. This would also enable a more complete comparison to be made with the continuum theory in the longitudinal field case.[14] For example, we could calculate the density of states and intensity distribution functions for the discrete SW modes within our model, and the continuum limit ($N\rightarrow\infty$ and $a\rightarrow 0$ such that Na^2 is constant) could then be studied. There would still be symmetry differences because we employ a hexagonal cross section, whereas the continuum theory[14] was for a circular cross section.

Notice that our formulation can be applied to nanowires with different size, shape, and lattice structure. In particular, the theory can be extended to other systems of ferromagnetic nanowires of arbitrary cross section. For example, we can choose to model a nanowire having a rectangular cross section, where the spins are arranged on a square lattice. This model can be used to study SW excitations in ferromagnetic stripes. These kind of structures have been fabricated and studied extensively in recent years by many experimental groups. It should be remarked that, *within a continuum approximation*, the problem of calculating a SW dispersion relation for a long ferromagnetic wire of rectangular cross section has never been solved analytically, not even in the magnetostatic limit.[2,21]

Another potential application of our theory is that it can straightforwardly be extended to more exotic structures such as arrays of long ferromagnetic nanotubes and even to finite-length nanorings. In the latter case, the nanorings fabricated so far[5,25] have length-to-diameter aspect ratios that can be as large as 5 in suitable cases, and therefore one would additionally need to take into account the end effects in these structures.

The theory can also be extended to incorporate the effects of interwire dipolar interactions in a dense array of ferromagnetic nanowires. We note that in the longitudinal case, where the wires have magnetization parallel to their symmetry axis, this problem has been addressed by Arias and Mills[15] using a continuum model. The authors have provided numerical examples for a pair of ferromagnetic cylindrical wires and a linear array. In the latter case, the results show a new dispersive mode which crosses and hybridizes with the modes of an individual nanowire. However, it is nontrivial to extend their theory to the transverse-field case, where the magnetization in each wire is nonuniform. Also, their theory does not apply to other systems with different geometry, such as arrays of magnetic stripes. In the present work we have discussed some preliminary results for finite arrays of nanowires in both longitudinal and transverse field, where each wire is represented by a long single line of spins and is arranged in a triangular lattice. However, it would be of interest to make further studies of such systems.

ACKNOWLEDGMENTS

We would like to acknowledge partial support from NSERC of Canada.

APPENDIX A

The coefficients $A^{(2)}_{n,m}(k)$ and $B^{(2)}_{n,m}(k)$ in the transverse case are given by

$$A^{(2)}_{n,m}(k) = \Delta_n \delta_{n,m} - \frac{1}{2} S J_{n,m}(k)\{\cos(\theta_n - \theta_m) + \sin\alpha_n \sin\alpha_m + \cos(\theta_n - \theta_m)\cos\alpha_n \cos\alpha_m + i\cos(\theta_n - \theta_m)(\cos\alpha_n + \cos\alpha_m)\}$$
$$+ \frac{1}{2}(g\mu_B)^2 S\{D^{x,x}_{n,m}(k)[\sin\theta_n \cos\alpha_n \sin\theta_m \cos\alpha_m + \cos\theta_n \cos\theta_m + i(\cos\theta_n \sin\theta_m \cos\alpha_m - \sin\theta_n \cos\alpha_n \cos\theta_m)]$$
$$+ D^{y,y}_{n,m}(k)\sin\alpha_n \sin\alpha_m + D^{z,z}_{n,m}(k)[\cos\theta_n \cos\alpha_n \cos\theta_m \cos\alpha_m + \sin\theta_n \sin\theta_m + i(\cos\theta_n \cos\alpha_n \sin\theta_m$$
$$- \sin\theta_n \cos\theta_m \cos\alpha_m)] + D^{x,z}_{n,m}(k)[\sin(\theta_n + \theta_m)(\cos\alpha_n \cos\alpha_m - 1) - i(\cos\alpha_n - \cos\alpha_m)\cos(\theta_n + \theta_m)] - D^{x,y}_{n,m}(k)$$
$$\times[\sin\theta_n \cos\alpha_n \sin\alpha_m + \sin\alpha_n \sin\theta_m \cos\alpha_m + i(\cos\theta_n \sin\alpha_m - \sin\alpha_n \cos\theta_m)] - D^{y,z}_{n,m}(k)[\cos\theta_n \cos\alpha_n \sin\alpha_m$$
$$+ \sin\alpha_n \cos\theta_m \cos\alpha_m + i(\sin\alpha_n \sin\theta_m - \sin\theta_n \sin\alpha_m)]\}, \tag{A1}$$

$$B^{(2)}_{n,m}(k) = -\frac{1}{4} S J_{n,m}(k)\{\cos(\theta_n - \theta_m)(\cos\alpha_n \cos\alpha_m - 1) + \sin\alpha_n \sin\alpha_m + i(\cos\alpha_n - \cos\alpha_m)\sin(\theta_n - \theta_m)\} + \frac{1}{4}(g\mu_B)^2 S\{D^{x,x}_{n,m}(k)$$
$$\times[\sin\theta_n \cos\alpha_n \sin\theta_m \cos\alpha_m - \cos\theta_n \cos\theta_m + i(\cos\theta_n \sin\theta_m \cos\alpha_m + \sin\alpha_n \cos\alpha_n \cos\theta_m)] + D^{y,y}_{n,m}(k)\sin\alpha_n \sin\alpha_m$$
$$+ D^{z,z}_{n,m}(k)[\cos\theta_n \cos\alpha_n \cos\theta_m \cos\alpha_m - \sin\theta_n \sin\theta_m - i(\sin\theta_n \cos\theta_m \cos\alpha_m + \cos\theta_n \cos\alpha_n \sin\theta_m)] + 2D^{x,z}_{n,m}(k)$$
$$\times[\sin\theta_n \cos\alpha_n \cos\theta_m \cos\alpha_m + \cos\theta_n \sin\theta_m + i(\cos\theta_n \cos\theta_m \cos\alpha_m - \sin\theta_n \cos\alpha_n \sin\theta_m)] - 2D^{x,y}_{n,m}(k)$$
$$\times[\sin\theta_n \cos\alpha_n \sin\alpha_m + i\cos\theta_n \sin\alpha_m] - 2D^{y,z}_{n,m}(k)[\sin\alpha_n \cos\theta_m \cos\alpha_m - i\sin\alpha_n \sin\theta_m]\}, \tag{A2}$$

where

$$\Delta_n = g\mu_B H_0 \cos\theta_n \sin\alpha_n + \sum_l \{S J_{n,l}(0)[\cos(\theta_n - \theta_l)\sin\alpha_n \sin\alpha_l + \cos\alpha_n \cos\alpha_l] - (g\mu_B)^2 S[D^{x,x}_{n,l}(0)\sin\theta_n \sin\alpha_n \times \sin\theta_l \sin\alpha_l$$
$$+ D^{y,y}_{n,l}(0)\cos\alpha_n \cos\alpha_l + D^{z,z}_{n,l}(0)\cos\theta_n \sin\alpha_n \cos\theta_l \sin\alpha_l + D^{x,z}_{n,l}(0)\sin(\theta_n + \theta_l)\sin\alpha_n \sin\alpha_l]\}. \tag{A3}$$

[1] *Spin Dynamics in Confined Magnetic Structures I*, edited by B. Hillebrands and K. Ounadjela (Springer Verlag, Berlin, 2002).
[2] S. O. Demokritov, B. Hillebrands, and A. N. Slavin, Phys. Rep. **348**, 441 (2001).
[3] G. Gubbiotti, P. Candeloro, L. Businaro, E. Di Fabrizio, A. Gerardino, R. Zivieri, M. Conti, and G. Carlotti, J. Appl. Phys. **93**, 7595 (2003).
[4] G. Gubbiotti, G. Carlotti, R. Zivieri, F. Nizzoli, T. Okuno, and T. Shinjo, J. Appl. Phys. **93**, 7607 (2003).
[5] Wentao Xu, D. B. Watkins, L. E. Delong, K. Rivkin, J. B. Ketterson, and V. V. Metlushko, J. Appl. Phys. **95**, 6645 (2004).
[6] A. Fert and L. Piraux, J. Magn. Magn. Mater. **200**, 338 (1999).
[7] K. Nielsch, F. Müller, A. P. Li, and U. Gösele, Adv. Mater. (Weinheim, Ger.) **12**, 582 (2000).
[8] K. Nielsch, R. B. Wehrspohn, J. Barthel, J. Kirschner, U. Gösele, S. F. Fischer, and H. Kronmüller, Appl. Phys. Lett. **79**, 1360 (2001).
[9] J. L. Duvail, S. Dubois, L. Piraux, A. Vaurès, A. Fert, D. Adam, M. Champagne, F. Rousseaux, and D. Decanini, J. Appl. Phys. **84**, 6359 (1998).
[10] A. Encinas-Oropesa, M. Demand, L. Piraux, I. Huynen, and U. Ebels, Phys. Rev. B **63**, 104415 (2001).
[11] U. Ebels, J. L. Duvail, P. E. Wigen, L. Piraux, L. D. Buda, and K. Ounadjela, Phys. Rev. B **64**, 144421 (2001).
[12] Z. K. Wang, M. H. Kuok, S. C. Ng, D. J. Lockwood, M. G. Cottam, K. Nielsch, R. B. Wehrspohn, and U. Gosële, Phys. Rev. Lett. **89**, 027201 (2002).
[13] T. M. Sharon and A. A. Maradudin, J. Phys. Chem. Solids **38**, 977 (1977).
[14] R. Arias and D. L. Mills, Phys. Rev. B **63**, 134439 (2001).
[15] R. Arias and D. L. Mills, Phys. Rev. B **67**, 094423 (2003).
[16] K. Yu. Guslienko and A. N. Slavin, J. Appl. Phys. **87**, 6337 (2000).
[17] K. Yu. Guslienko and A. N. Slavin, J. Magn. Magn. Mater. **215**, 576 (2000).
[18] R. N. Costa Filho, M. G. Cottam, and G. A. Farias, Phys. Rev. B **62**, 6545 (2000).
[19] J. M. Pereira and M. G. Cottam, Phys. Rev. B **68**, 104429 (2003).
[20] R. M. White, M. Sparks, and I. Ortenburger, Phys. Rev. **139**, A450 (1965).
[21] A. G. Gurevich and G. A. Melkov, *Magnetization Oscillations and Waves* (CRC Press, New York, 1996).
[22] M. G. Cottam and D. R. Tilley, *Introduction to Surface and Superlattice Excitations*, 2nd ed. (IOP, Bristol, 2005).
[23] R. L. Stamps and B. Hillebrands, Phys. Rev. B **43**, 3532 (1991).
[24] R. L. Stamps and B. Hillebrands, Phys. Rev. B **44**, 5095 (1991).
[25] K. L. Hobbs, P. R. Larson, G. D. Lian, J. C. Keay, and M. B. Johnson, Nano Lett. **4**, 167 (2004).